Reactivity of fatty acid methyl esters under atmospheric pressure plasma jet exposure: An experimental and theoretical study

(Article begins on next page)

07 January 2023

Luca Matteo Martini, Andrea Maranzana, Glauco Tonachini, Giulia Bortolotti, Marco Scapinello, Mario Scotoni, Graziano Guella, Giorgio Dilecce, Paolo Tosi

Reactivity of fatty acid methyl esters under atmospheric pressure plasma jet exposure: An experimental and theoretical study.

Reactivity of Fatty Acid Methyl Esters under Atmospheric Pressure Plasma Jet Exposure. An Experimental and Theoretical Study

Luca Matteo Martini[*1], Andrea Maranzana[2], Glauco Tonachini[2], Giulia Bortolotti[1], Marco Scapinello[†1], Mario Scotoni[1], Graziano Guella[1], Giorgio Dilecce[1,3], and Paolo Tosi[1]

[1]Department of Physics, University of Trento, via Sommarive 14, Trento I-38123, Italy
[2]Dipartimento di Chimica, Università di Torino, Corso Massimo D'Azeglio 48, I-10125 Torino, Italy
[3]CNR NANOTEC - PLasMI Lab., via Amendola 122/D, I-70126 Bari, Italy

6th March 2017

Abstract

We have investigated the treatment of a mixture of fatty acid methyl esters by an RF-plasma jet with He-H_2O and He-O_2 gas feed. We have measured the concentration of the hydroxyl radical in the jet by laser induced fluorescence, looking for correlation with the lipid reactivity. We have detected four product families, whose yields increase with the OH exposure: volatile products, polymerization products, reduced chains and oxidised chains. Theoretical calculations give insights on the radical attack to the lipid chain and show that none of the products can be attributed exclusively to reactions with OH. Therefore, the observed reactant conversion as function of the OH exposure must be interpreted as a qualitative relationship with the total amount of radical species present in the plasma jet.

1 Introduction

Lipids are key metabolites with a huge variety of biological roles since they can act as energy reservoirs, structural components of cell membranes and signalling molecules.[1,2] Their oxidation is associated with various human diseases and consequently, the topic of

---

[*]luca.martini.1@unitn.it

[†]*present address:* Chemical Engineering Department, KU Leuven, Leuven, Belgium

the reactions between lipids and reactive oxygen species (ROS), which are produced during aerobic metabolism and by various enzymatic reactions, has become an important research area in life sciences. [3,4]

Besides biology, lipid oxidation is also important in combustion and atmospheric chemistry, [5] thus attracting interest from many different disciplines. Many studies have been conducted on autoxidation, [6-13] and with the addition of selected radicals. [14-16] However, the characterization of the products and their quantitative relationship with the various ROS are not fully understood yet. One of the reasons is that in many experiments ROS are generated by different ways, but are not quantified.

In the emerging field of Plasma Medicine, the interaction of active species produced by electrical discharges with living tissues, and in particular with lipids, is nowadays getting the attention of fundamental studies. [17-19] In this context, we have carried out an experiment in which a radio-frequency plasma-jet impinges on the surface of a liquid target, composed of fatty acid methyl esters (FAME), and triggers their conversion. The atmospheric pressure plasma jet (APPJ) is a kind of electrical discharge device particularly suited for biological applications of plasmas, that allows to generate reactive oxygen species (ROS), such as O_3, OH, O and $O_2(a^1\Delta_g)$ radicals with a remote discharge. [5,20,21] Although it does not generate selectively individual reactive oxygen species, it is possible to change drastically the relative abundance of OH on other ROS. Model calculations indicate that in He plus water plasmas, OH is the most abundant species, while other ROS, in particular O_3, O and $O_2(a^1\Delta_g)$ (non-OH ROS), have a factor of two/three lower concentration. [22] The addition of O_2 to the feed gas greatly enhances the production of O, O_3 and $O_2(a^1\Delta_g)$. [23] Air penetration in the jet plume attains a similar effect. [24] By changing the feed gas composition, we can thus select two extreme ROS relative abundances:

- with He-H_2O gas feed and very small air penetration, OH is about two times more abundant than the other non-OH ROS. We call this an OH rich condition;

- with He-O_2 gas feed, O, O_3 and $O_2(a^1\Delta_g)$ concentrations are more than one order of magnitude larger than that of OH. We refer to this as an non-OH ROS rich condition.

In our experiment, we have measured the concentration of OH by laser induced fluorescence (LIF) and estimated the flux of OH radicals to the surface. Such a measurement is a partial characterization of the radicals impinging on the surface and, as discussed later, a clear-cut, quantitative marker of the fundamental difference between the two gas feed conditions.

A conceptually similar study has been recently published. [25] In that work, an RF plasma jet fed with Ar-O_2 and Ar-H_2O mixtures was used to accelerate lipid oxidation, while O and OH concentrations were measured by two-photons absorption LIF (TALIF) and LIF respectively. Volatile oxidation products only were analysed. As in our case, the two mixtures generated non-OH ROS rich and OH rich conditions. In the first case, with measured O concentrations of the order of 10^{15} to $10^{16}\,\mathrm{cm^{-3}}$, a lot of volatile oxidation products were observed. In the OH rich conditions, instead, with OH densities in the jet of the order of 10^{12} to $10^{13}\,\mathrm{cm^{-3}}$ and a treatment time of 20 minutes, a very low amount of products was detected. Such a low oxidation rate was attributed to the low OH concentration, the latter being due to air diffusion into the effluent plasma jet. No attempt was made to correlate the O flux on the liquid surface to the volatile products quantitatively. Further studies by the same group focussed only on volatile oxidation products generated by non-OH ROS rich jets treatments. [26-28]

Unlike the work of ref [25] we have: a) treated directly a FAME mixture, obtained by transesterification of a seed oil mixture; b) analysed oxidation products in the liquid phase; c) obtained conditions of much higher OH concentrations close to the target surface, up to
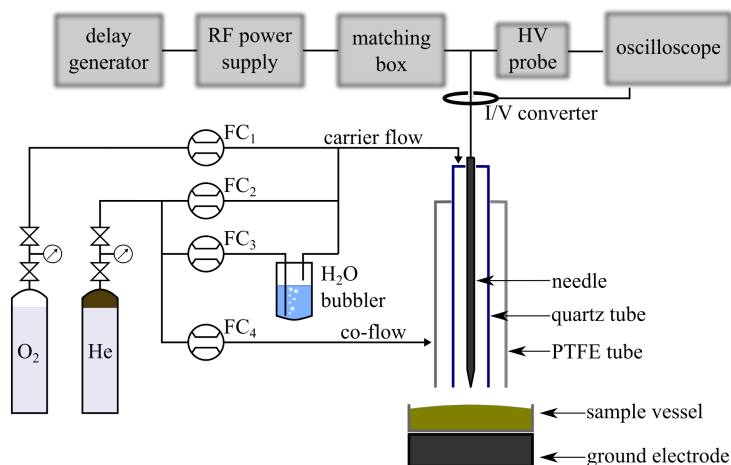
Figure 1: Schematic representation of the radio frequency plasma jet apparatus. $FC_{1,2,3,4}$: mass flow controllers; HV probe: high voltage probe.

$10^{14}\,cm^{-3}$, by a different ground electrode geometry and by a He co-flow that prevents air penetration into the effluent jet; d) calculated the OH flux from the concentration, measured by LIF, and the size/geometry of the jet at the target surface, measured by Schlieren imaging. The OH rich jet produces large amounts of products, mainly volatile oxidation products, oxidised chains, dimers and saturated chains. Since the radicals production in the jet is not selective, the choice of feeding the jet with the two different mixtures aims at unbalancing the relative abundances of oxidising species. The non-OH ROS rich jet is then studied as a condition qualitatively opposite to that of the OH rich case and to compare results with literature data.

The interaction of OH with lipids, namely its first step of hydrogen abstraction and O_2 addition to the allyl radical, has been already modelled.[29] The He-H_2O jet, however, does not contain OH only, but a blend of radicals where OH is the most abundant ROS, plus atomic hydrogen, H, that, according to the calculations of [22] can be one even order of magnitude more abundant than OH.

In a first attempt to understand the products of the He-H_2O jet treatment, theoretical calculations have been carried out, focussing on the initial reaction steps of unsaturated esters attack by OH, O and H. Reaction pathways initiated by the hydroxyl radical, then possibly involving dioxygen, are studied. They can bring about oxidation of the original systems to different extents, but can also produce non-oxidised species. Previous theoretical studies have focused on $O_2(^1\Delta_g)$ addition to a linoleic acid model, nona-3(cis),6(cis)-diene,[30] or on OH radical attack followed by $O_2(^3\Sigma_g^-)$ attack on the same model and on linoleic acid itself.[29] Particular aspects, as the allylperoxyl rearrangement (a reaction relevant to the spontaneous autoxidation of unsaturated lipids of biological interest), have also been dealt with.[31]

2 Experimental Section

2.1 Plasma jet

The plasma source (Figure 1) consists of a tungsten needle of $2\,mm$ diameter that acts as high voltage electrode, surrounded by a quartz tube ($3\,mm$ inner diameter, $5\,mm$ outer diameter) where He or a mixture of He-H_2O/He-O_2 flows. To prevent contamination of the plasma plume by the outside atmosphere, a PTFE tube ($6\,mm$ inner diameter, $7\,mm$ outer

diameter) concentric to the needle is used to inject a co-flow of pure He. The He-H_2O mixture was obtained by injecting a fraction of the gas carrier inside a bubbler filled with distilled water at $23\,°C$. Gas flows were controlled by using four mass flow controllers (1179A, MKS). Pure He (99.999 %) and oxygen (99.995 %) were used.

The grounded electrode (an aluminium cylinder of $20\,mm$ diameter) was placed $11(1)\,mm$ below the tungsten needle tip. The liquid target was placed inside a small PTFE cylindrical vessel above the grounded electrode (the distance between the target surface and plasma jet tip was $5(1)\,mm$).

An RF power supply (RF5S, RFPP) working at $13.56\,MHz$ generated the discharge. Impedance matching between the power supply and the plasma jet was achieved by using a matching network (AM5, RFPP). Voltage and current applied to the discharge were measured by a voltage probe (P6015A, Tektronix) and a high bandwidth ($200\,Hz$ to $500\,MHz$) I/V converter (CT-C1.0-B, Magnelab), respectively. Their signals were recorded and digitised by a digital oscilloscope (Wavesurfer 104MXs-A $1\,GHz$ $5\,GSps$, LeCroy). The power is calculated as

$$P = V_{rms}I_{rms}\cos\phi \qquad (1)$$

where ϕ is the phase shift between the voltage and the current, corrected for the time delay introduced by the acquisition system. This systematic error in the acquisition of the I-V characteristic is due to the time delay introduced by probes, cables, and the oscilloscope.[32] The power dissipated into the plasma is the difference between the power values, measured when the discharge is on and off, respectively.[33] The plasma power was continuously monitored and kept constant during each treatment.

The sample temperature (on the interface between the FAME and the plasma jet) was monitored with an infrared camera (T450sc, FLIR) and a temperature sensor (LM35, Texas Instruments) placed inside the grounded electrode.

2.2 OH detection

The LIF set-up is shown in Figure 2. It is composed of a dye laser (TDL50, Quantel with Rhodamine 590 chloride) pumped by a Q-switched Nd:YAG laser (YG580, Quantel). The dye laser was frequency doubled using a KDP crystal harmonic generator. The UV-beam energy at $2829\,Å$, after fundamental separation, was around $0.53\,mJ\,pulse^{-1}$. The energy of the beam was controlled by a variable optical attenuator based on Fresnel reflection. The attenuated beam was spatially filtered before being focussed by a f=$250\,mm$ lens, the beam waist inside the target area was around $80\,\mu m$. The energy of the laser beam was recorded by a single-channel silicon-based thermopile (DX-0576, Dexter research centre). The fluorescence signal was collected in the scatter arrangement by a f=$200\,mm$ lens and injected in the detection system by a f=$75\,mm$ lens. A Shamrock 303i $300\,mm$ focal length monochromator, equipped with two gratings ($1200\,gr\,mm^{-1}$ blaze $300\,nm$ and $600\,gr\,mm^{-1}$ blaze $300\,nm$) was used to separate the spectral components of the fluorescence signal. The monochromator was coupled with two different detectors: a 1024x1024 px intensified CCD (ICCD) (DH334T-18U-03, Andor) and a gateable photomultiplier tube (PMT) (8575, Burle Electron Tubes). The ICCD was used to record the spectrum of the fluorescence signal, while the PMT served to record the temporal evolution of the LIF signal. We adopted the classical excitation-detection scheme that involves transitions of the $3064\,Å$ system:

$$OH(X^2\Pi, v=0) + h\nu_L \rightarrow OH(A^2\Sigma^+, v=1,0) \rightarrow OH(X^2\Pi, v=1,0) + h\nu \quad (2)$$
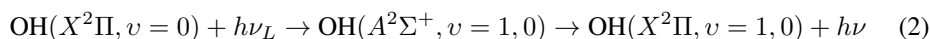
The details on LIF outcomes analysis and calibration are described in a previous work.[34]

To measure the number of OH radicals hitting the target, we performed LIF measurements $0.5\,mm$ above the sample vessel. The outcome of LIF measurement is the OH density inside
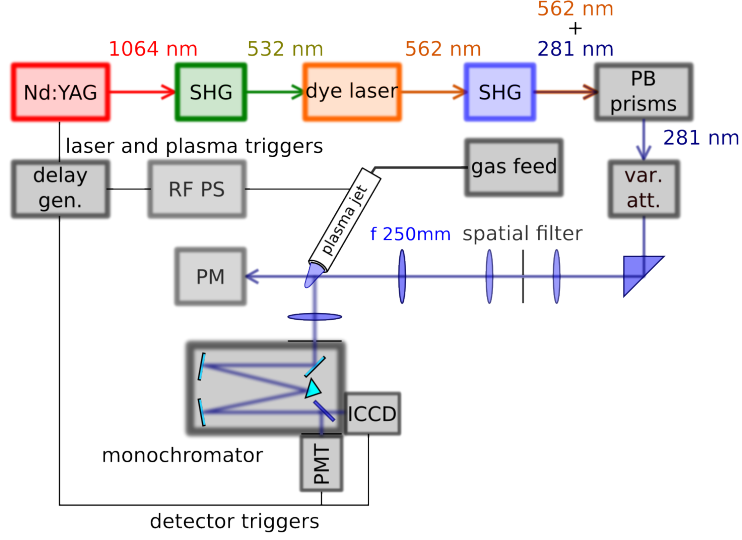
Figure 2: Schematic representation of the LIF experimental setup. SHG: second harmonic generator; PB prisms: fundamental separator; var. att.: variable optical attenuator; PM: thermopile-based energy detector; ICCD: intensified CCD; PMT: photomultiplier tube; RF PS: radio-frequency power supply.

the sampled volume, roughly a cube of $\simeq 0.2 \times 0.2 \times 0.2 \, \mathrm{mm}^3$ volume, whose projection on the target plane is about $0.04 \, \mathrm{mm}^2$. The area of the target hit by the plasma jet was much larger ($\simeq 0.3 \, \mathrm{mm}^2$). Thus the determination of the OH radical distribution over the sample requires the collection of a large number of measurements that is much more time consuming than a typical treatment ($270 \, \mathrm{min}$). For this reason, we characterised the plasma jet OH density profile once taking around 60 points every $\simeq 0.5 \, \mathrm{mm}$. The result is shown in Figure 3 where the data were interpolated via cubic algorithm. We verified that the OH density could be considered distributed according to a cylindrical symmetry. Under this assumption, during each treatment we measured the radial OH distribution $[\mathrm{OH}] \, (r)$ by averaging the OH density collected along four radii, starting from the maximum of the OH density distribution, taken at $\pi/2$ each other.

We estimate the exposure $\mathrm{E_{OH}}$ (i.e. the total number of OH radicals that impinges on the target) by assuming that the source has a constant OH production during treatment time and a cylindrical symmetry. The exposure is given by:

$$E_{\mathrm{OH}} = t \cdot \xi_{\mathrm{OH}} = t \cdot \frac{\Phi}{\pi r^2} \cdot \iint_{S_T} [\mathrm{OH}] \left(\sqrt{x^2 + y^2} \right) \mathrm{d}x\mathrm{d}y, \qquad (3)$$

where t is the treatment time, ξ_{OH} is the OH flux (i.e. the number of OH particles that reaches the target in the unit of time), Φ is the plasma jet total flux (carrier plus co-flow), r is the radius described by the flow exiting the plasma jet and S_T is the surface where the OH is calculated. The origin of the Cartesian system of coordinates is where the OH density has the largest value. The jet flow was kept fixed at $4.3(1) \times 10^3$ sccm and the radius r described by the jet flow over the sample was estimated in $3.8(2) \, \mathrm{mm}$ by schlieren imaging. The error connected to the OH exposure is mainly due to fluctuations of the plasma source and to the non-uniformity of the OH profile. The relative error on OH exposure has been estimated at $10 \, \%$.
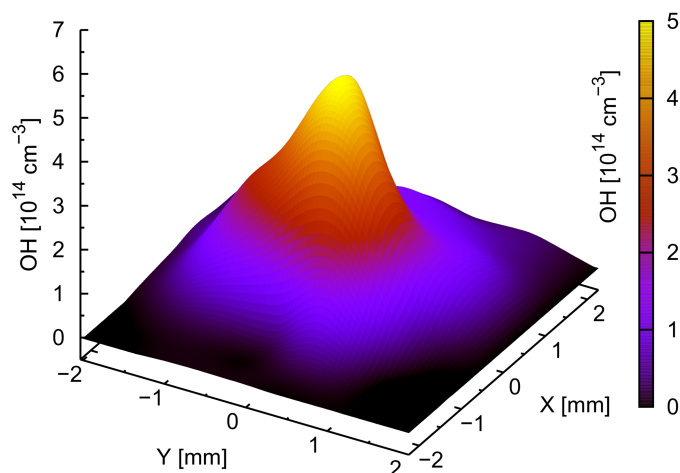
5

Figure 3: 3D map of OH in the effluent jet impinging on the FAME target. The map was recorded $0.5\,\mathrm{mm}$ above the target. The map is made of around 60 interpolated experimental points. The effluent carrier flux was $2.15(7) \times 10^3\,\mathrm{sccm}$ (helium $99.36\,\%$ and water $0.64\,\%$), co-flow was $2.15(7) \times 10^3\,\mathrm{sccm}$ (pure helium). The plasma jet power was $0.98(5)\,\mathrm{W}$. OH flux was $2.8(3) \times 10^{15}\,\mathrm{s^{-1}}$.

2.3 Products determination

2.3.1 Gas chromatography

The samples were analysed by chromatographic techniques. Gas chromatography was performed by using a GC with FID detector (Trace GC Ultra, Thermo Finningan) for quantitative information and MS detector (Trace DSQ, Thermo Finningan) for qualitative information. The method was developed to evaluate several classes of compounds, not for the best separations of a unique class of compounds. The column was a DB-5MS (J&W Scientific), $60\,\mathrm{m}$ length, $0.25\,\mathrm{mm}$ diameter, $0.25\,\mathrm{\mu m}$ film width. The temperature program was: $50\,^{\circ}\mathrm{C}$, $4\,\mathrm{min}$; $140\,^{\circ}\mathrm{C}$, $15\,^{\circ}\mathrm{C\,min^{-1}}$; $200\,^{\circ}\mathrm{C}$, $4\,^{\circ}\mathrm{C\,min^{-1}}$; $230\,^{\circ}\mathrm{C}$, $1.5\,^{\circ}\mathrm{C\,min^{-1}}$; $300\,^{\circ}\mathrm{C}$, $10\,^{\circ}\mathrm{C\,min^{-1}}$; $300\,^{\circ}\mathrm{C}$, $48\,\mathrm{min}$. The carrier gas was helium, at a flow of $2.5\,\mathrm{ml\,min^{-1}}$, the injector was heated at $260\,^{\circ}\mathrm{C}$ and a split ratio of 10 was chosen. The sample was obtained dissolving $5.0\,\mathrm{\mu l}$ of untreated/treated FAME in $1.0\,\mathrm{ml}$ of hexane and adding $50.0\,\mathrm{\mu l}$ of internal standard (IS) solution (ethyl isovalerate $6.5\,\mathrm{g\,ml^{-1}}$ and methyl myristate $6.4\,\mathrm{g\,ml^{-1}}$). The injected volume in the GC was $1\,\mathrm{\mu l}$. IS was introduced to normalize the syringe injection contribute. Quantitative data were obtained by using FID chromatographic areas and dividing them by the effective carbon numbers. These were calculated by taking into account the molecular formula as obtained by MS spectra.[35]

2.3.2 Nuclear Magnetic Resonance

^{1}H- ($400\,\mathrm{MHz}$) and ^{13}C-NMR ($100\,\mathrm{MHz}$) spectra were recorded in deuterated chloroform (99.90% CDCl$_3$) at $300\,\mathrm{K}$ on a Bruker-Avance $400\,\mathrm{MHz}$ NMR spectrometer by using a $5\,\mathrm{mm}$ BBI probe equipped with pulsed-gradient field utility. The chemical shift scale (δ) was calibrated on the residual proton signal of CDCl$_3$ at δ_H $7.26\,\mathrm{ppm}$ whilst the ^{13}C-NMR scale was calibrated on the resonance of the C carbon signal of the solvent at δ_C $77.00\,\mathrm{ppm}$. The following experiments were done (info obtained are reported in brackets): ^{1}H-NMR (proton chemical shifts and scalar couplings J); ^{1}H-^{1}H COSY (proton-proton scalar correlation); ^{1}H- ^{13}C HSQC (proton-carbon one-bond correlation); ^{1}H- ^{13}C HMBC (proton-carbon
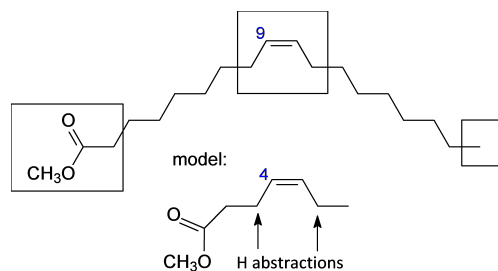
6

Figure 4: The oleate model X. The model methyl-*cis*-hept-4-enoate is built from selected parts of methyl-*cis*-octadec-9-enoate (methyl oleate). The purpose is to preserve the chief structural traits of the oleate molecule, while reducing significantly the oleate conformational richness.
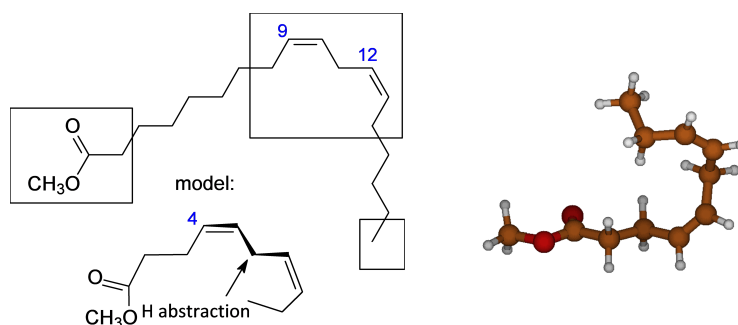

Figure 5: Left: the linoleate model Y, the model methyl-*cis*,*cis*-deca-4,7-dienoate is built from selected parts of methyl-*cis*,*cis*-octadec-9,12-dienoate (methyl linoleate). Right: the most stable explored conformations of the model ester (non-planar).

multiple-bond correlation). 1D NMR spectra were integrated by the software MestreNova 9.1 (Mestrelab Research S.L., Escondido, CA).

2.4 Theoretical Method

The reaction studied experimentally involves methyl oleate (methyl *cis*-octadec-9-enoate) and methyl linoleate (methyl-*cis*,*cis*-octadec-9,12-dienoate). They presumably can react on the one hand with some oxidising species, namely the radical $OH(X^2\Pi_{3/2})$, and the diradical $O(^3P)$, and also with both ground and excited state molecular oxygen, $O_2(X^3\Sigma_g^-)$ and $O_2(a^1\Delta_g)$, respectively. On the other hand, also hydrogen atoms are present. In the computational part, oleate is modeled by methyl-*cis*-hept-4-enoate ("oleate model"), linoleate by methyl-*cis*,*cis*-deca-4,7-dienoate ("linoleate model"). Moreover, the reactions considered are limited, for feasibility reasons, to the hydroxyl radical, ground state oxygen and hydrogen atoms, as well as dioxygen. The criteria adopted to choose the model molecules (i.e. maintaining the essential traits of the two structures while avoiding a plethora of conformationally stable structures) are shown pictorially in Figure 4, for the oleate, and in Figure 5, for the linoleate. Within this limited model, stable and transition structures (TS), corresponding to minima and first order saddle points on the energy hypersurface, are determined by Density Functional Theory (DFT) [36] using the M06-2X functional [37] and gradient procedures. [38-42] Dunning's polarised valence-3ζ cc-pVTZ basis set [43] is used in the DFT optimizations, and the nature of the critical points is checked by vibrational analysis. The overall theory level, DFT(M06-2X)/cc-pVTZ//DFT(M06-2X)/cc-pVTZ, is expected to perform acceptably on the basis of previous studies. [44,45]

Since the experimentally studied fatty acid methyl esters are in the liquid phase, the re-

acting molecules are considered as a solute in a polarised continuum, within the SMD [46] and IEF-PCM [47] schemes [1]. Therefore, the reactions are seen as taking place in the liquid phase, upon diffusion in it, to some degree, of the small reacting species OH , H, O, and O_2 (also reaction in significant part at the interface would be conceivable). The dielectric constant was set on the basis of literature values [48,49] as ε=3.20, while ε_{inf}=2.158. The liquid phase reasonably ensures fast thermalization of the reacting systems.

In detail, the thermochemical corrections gave estimates of the relative Gibbs free energies (ΔG) were estimated (within the usual approximations) [50-52] for T=353 K and are reported in the Figure 9, 10, 14 and 17. Estimates of the rate constants for each step are reported in the Supporting Information. Because we consider all species in thermal equilibrium with the surrounding medium, we discuss in the text each $\Delta G^{\ddagger}$ barrier with respect to the preceding minimum, and compute the kinetic constants by the TST approach. [53-56] In the case of the transition structures for dioxygen addition to a radical species (overall spin multiplicity is doublet, $\hat{S}^2$=0.75), significant spin contamination is observed ($\hat{S}^2$ values in the 1.13-1.37 range). For that reason, the energy values were refined by removing the quartet contribution by Yamaguchi's formula. [57,58] Quantum mechanical calculations were carried out by using the GAUSSIAN09 system of programs. [59]

3 Results

3.1 Experimental results

The untreated sample was a mixture of FAME, obtained by transesterification in acid catalytic condition of a commercial oilseed mixture. The main components of the initial FAME mixture are unsaturated FAME $C18_U^i$ 89(3) % (methyl oleate C18:1, methyl linoleate C18:2 and methyl linolenate C18:3) and saturated FAME 9.9(5) % (methyl palmitate C16:0 6.9(3) %, methyl stearate C18:0 3.0(2) %). We have exposed 100 µl of FAME to the plasma-jet plume, by using three types of discharge:

- pure helium discharge with a plasma power of 2.7(3) W; it produces a very low ROS concentration (OH flux less than $6.2(4) \times 10^{14}\,\text{s}^{-1}$), essentially due to residual water in the gas feed line;

- helium (99.25 %) and oxygen (0.75 %) discharge with a plasma power of about 2.4(3) W; it produces an non-OH ROS flux at least one order of magnitude larger than the OH residual flux ($6.2(4) \times 10^{14}\,\text{s}^{-1}$);

- helium (99.36 %) and water (0.64 %) discharge operating at 2.0(2) W, 1.4(1) W and 0.98(5) W. It produces an OH flux of $5.5(5) \times 10^{15}\,\text{s}^{-1}$, $3.4(3) \times 10^{15}\,\text{s}^{-1}$ and $2.8(3) \times 10^{15}\,\text{s}^{-1}$, respectively. The air penetration inside the jet plume was monitored by analysis of OH LIF quenching. [34] Oxygen content inside the plume was lower than 0.1 %. In this condition non-OH ROS flux is at least two times lower than OH one.

Typical treatment times were 90, 180 and 270 min. The sample temperature measured with the infrared camera never exceeded 80(5) °C. Reaction products were analysed by GC-MS, GC-FID, and NMR spectroscopy.

---

[1] In the Solvation Model SMD ("D" stands for "density" because the full solute electron density is used) the solvent is represented as a dielectric medium. SMD separates the observable solvation free energy into two main components: a) the bulk electrostatic contribution arising from a self-consistent reaction field treatment; b) the cavity-dispersion-solvent-structure term and is the contribution arising from short-range interactions between the solute and solvent molecules in the first solvation shell. On the other hand, IEF is an integral equation formalism that treats on the same ground linear isotropic solvent models, anisotropic liquid crystals, and ionic solutions.
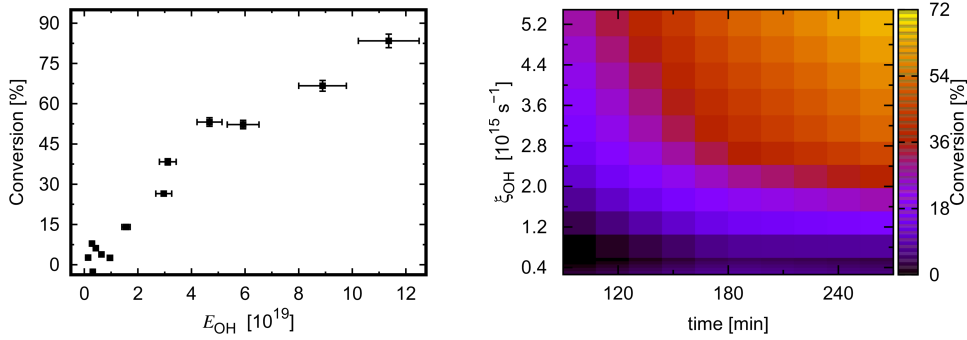
Figure 6: Left: conversion of unsaturated FAMEs $C18_U^i$ versus OH exposure E_{OH}; Right: conversion of $C18_U^i$ versus treatment time and OH flux ξ_{OH}.

3.2 OH rich plasma

In the case of OH rich plasma (He and He and water discharge) we identified four classes of products:

- Volatile oxidation products: these can be primary or secondary products. The main detected compounds are aldehydes (n-hexanal and n-nonanal) and methyl-oxo-esters (9-oxo-nonanoate and 10-oxo-nonanoate). Their signal in the GC chromatogram might be explained either by their effective presence in the sample or by the thermal degradation of organic peroxides. Among these compounds, the most relevant are aldehydes (as n-nonanal), FAMEs (as methyl octanoate) and oxo-FAMEs (as methyl 9-oxo-nonanoate) as already reported in the literature. [6]

- "dimers": these products result from the coupling of two reactant FAMEs, either with or without oxygen (but not as peroxide). These species are similar to those reported by other groups. [60]

- reduced C18 chains, which are attributed to the saturation of the original C=C double bonds, likely by H radicals.

- oxidised C18 chains, such as 9-epoxy methyl oleate, 9-oxo methyl-oleate, and 9- and 10-hydroxy-metilstearate.

The reactants conversion as a function of the OH flux was investigated by treating samples at different RF powers and treatment durations. The samples were analyzed by chromatography. Since the outcome of a FID chromatogram is a relative concentration, a normalization to a constant amount is needed. To this purpose, we used the signal of the C16:0 FAME that, being it a saturated compound and then much less reactive than unsaturated ones, [61] can be safely taken as a constant reference. In addition, we have grouped together the signals of unsaturated C18 chains, due to partial overlapping of their peaks in the FID chromatogram. $C18_U^i$ is then the integrated signal of C18:1, C18:2 and C18:3.

The conversion of unsaturated FAMEs present in the sample, $C18_U^i$, is calculated as:

$$\text{Conversion} = \frac{n^i_{C18_U} - n^f_{C18_U}}{n^i_{C18_U}} \cdot 100, \qquad (4)$$

where $n^i_{C18_U}$ and $n^f_{C18_U}$ are the mole numbers of the unsaturated FAMEs before and after the treatment, respectively. Results are reported in Figure 6, in which the conversion is plotted
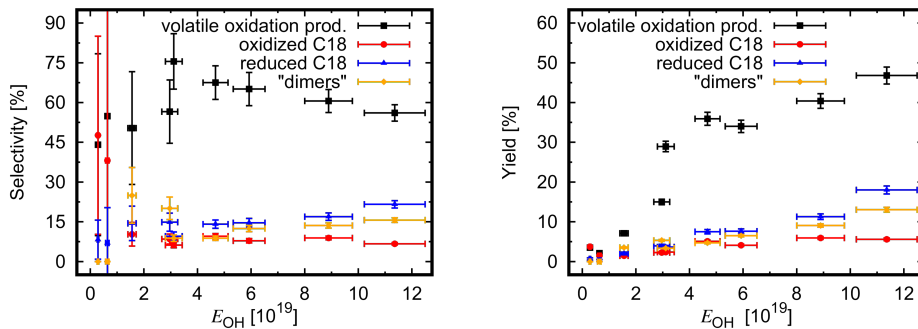
9

Figure 7: Selectivity (left) and Yield (right) of the four classes of products (volatile oxidation products, oxidised C18, reduced C18 and dimers) versus OH exposure E_{OH}.

against both the OH exposure and of the treatment time. The meaning of such a plot will be made clear in the discussion.

Yield and selectivity are defined as:

$$\text{Selectivity}_x = \frac{n_x^f}{n_{C18_U}^i - n_{C18_U}^f} \cdot 100, \tag{5}$$

$$\text{Yield}_x = \frac{n_x^f}{n_{C18_U}^i} \cdot 100. \tag{6}$$

Yield and selectivity were calculated for the four classes of products detected, and are shown in Figure 7. As an example, at $53(1)\,\%$ conversion, we estimate that $29.7(8)\,\%$ of the sample, corresponding to $61(3)\,\%$ of the products, was lost during treatment. These un-collected products are likely light compounds which evaporate and are lost due to the high He flux. Selectivities are $66(6)\,\%$ for volatile oxidation products, $14(2)\,\%$ for reduced C18 chains, $10(1)\,\%$ for "dimers" and $9(1)\,\%$ for oxidised C18 chains. The yields are $35.0(2)\,\%$, $7.6(4)\,\%$, $6(1)\,\%$ and $4.6(7)\,\%$, respectively.

The NMR analysis, carried out on FAME samples after plasma treatment in the OH-rich conditions, showed that unsaturated FAMEs almost disappeared (strong decrease of the olefinic signal centered at $5.37\,\text{ppm}$); in particular the ^{1}H-NMR spectrum (Figure 8) showed a complete disappearance both of the signal due to bis-allylic methylene at $2.78\,\text{ppm}$ of polyunsaturated FAME (18:2+18:3) and of the signal due to the terminal methyl at $0.97\,\text{ppm}$ of the α-linolenic acyl chain. Only residual amount of monounsaturated lipid species (residual olefinic protons at 5.37, allylic protons at $2.04\,\text{ppm}$) survived to this treatment. Worth of note, epoxide-containing lipid species, as established by the presence of small signals at 2.89 and $2.65\,\text{ppm}$ coupled to carbon resonances at 57.5 and $59.1\,\text{ppm}$, were the only oxidised species detectable in our NMR spectra, being NMR signals due to aldehyde or peroxide lipids very low or almost undetectable.

3.3 non-OH ROS rich plasma

In the case of the He-O_2 plasma (non-OH ROS rich), we observed an enhanced reactivity since also saturated FAMEs reacted. Consequently, due to the lack of the normalisation factor we could not define the conversion. We detected volatile oxidation products and ox-idised products. Both are formed by autoxidation processes, via the initial formation of the peroxyl radical. Volatile products likely derive from the decomposition of organic peroxides
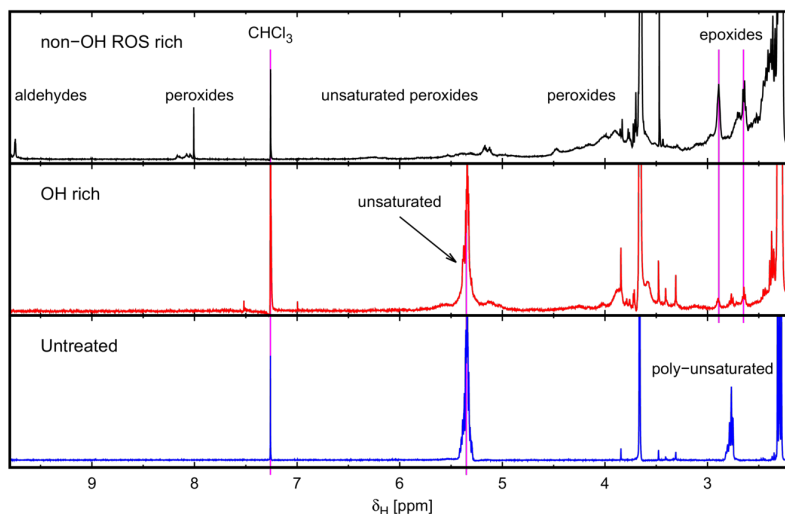
Figure 8: ^{1}H NMR spectra in CDCl$_3$ (300 K) of untreated FAME (bottom), FAME treated by OH-rich plasma (medium) and FAME treated by ROS rich plasma (top). Functional groups annotation according to the characteristic chemical shifts of the corresponding ^{1}H-NMR signals.

and hydroperoxides. We recognised several fragments, derived from the alkylic part, as aldehydes (hexanal, heptanal, 2-heptenal, octanal, nonanal, 2-nonenal and 3-nonenal, decanal, 2-decenal, 4,4-decadienal); alkanes and alkenes (octane, octene); alcohols (pentanol, octen-1-ol); carboxylic acids (nonanoic acid) and others deriving by the esteric part, such as methyl esters (methyl heptanoate, methyl octanoate, methyl nonanoate), oxo-methylesters (8-oxo methyl octanoate, 9-oxo methyl nonanoate, 10-oxo methyl decanoate, 10-oxo methyl-8- decenoate, 11-oxo methyl 9-undecenoate) and others (8-hydroxy-methyl octanoate, 9-hydroxy-methyl - 8 - nonanoate, 9-oxo-methyl decanoate, 6,8-dioxo-methyl nonanoate, 9-carboxy-methyl nonanoate). Oxidised products derive from the methyl oleate and the methyl linoleate. We have unambiguously detected 9-epoxy methyl oleate, 9-oxo methyl-oleate, 9- and 10-hydroxy-methyl stearate. Other oxygenated compounds were also detected, but their nature is not clearly identified, due to the presence of several isomers with similar retention times in the MS chromatogram.

Compared to the OH-rich case, we find almost the same products: aldehydes, alchohols, methyl esters and oxo-methyl esters. Only the appearance of some carboxylic acids and carboxy-methyl esters is peculiar of the non OH-rich treatment.

The NMR analysis, carried out on FAME samples after plasma treatment in the O$_2$ feed plasma conditions, showed the complete disappearance of unsaturated FAMEs (olefinic signal centered at 5.37 ppm). On the other hand, a huge relative amount of oxidised products were clearly detected. Among them, free aldehydes (singlet signals at 9.75 and 9.54 ppm, aldehydic protons), hydroperoxides (series of multiplets at 8.04-8.15 ppm, -OOH protons) and epoxides (signals at 2 .89 and 2 .65 ppm) were clearly detected.

3.4 Theoretical results

The hydroxyl radical can either give radical addition to the double carbon-carbon bonds or operate an H abstraction from a suitable position. For the oleate model shown in Figure 4, both possible additions to the C=C bonds are considered, together with those H abstractions from the methylene groups adjacent to the C=C (arrows), which are apt to form an allyl radical
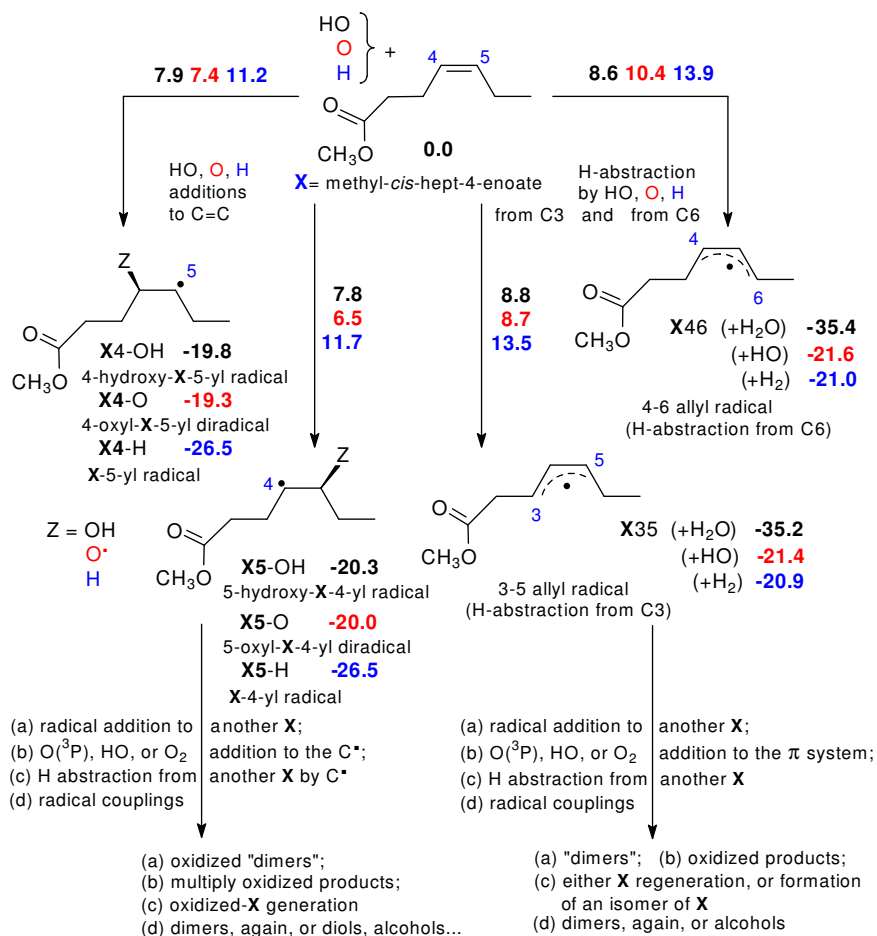
11

Figure 9: Left: Hydroxyl (black figures), oxygen atom (red figures), and hydrogen atom (blue figures) addition to the C=C bond of methyl *cis*-hept-4-enoate (X) producing the localised radicals: X4-OH, with OH on C4, and X5-OH, with OH on C5. Right: H abstraction (same colour code) from C3 or C6, producing the allyl radicals X46 and X35, respectively. Bottom: possible further reaction steps and products

system in the resulting intermediate product. Four transition structures and four resulting intermediates are consequently optimised for the initial step upon hydroxyl attacks.

For the linoleate model shown in Figure 5, the only process studied is bis-allylic H abstraction (i.e. from that methylene group which lies between the two C=C bonds: arrow). This reaction step is new with respect to the previous case because it generates a pentadienyl radical instead of an allyl radical. The other conceivable attacks (additions or H abstractions) would be, on the other hand, quite similar to those considered for the oleate, and do not seem to be worthwhile of an extension of the study.

3.4.1 The "oleate model": initial reaction steps.

Hydroxyl, atomic oxygen and hydrogen attacks. In methyl *cis*-hept-4-enoate (X), •OH addition to either carbon of the C=C bond (numbered 4 or 5) gives the localised radicals X4-OH and X5-OH (Figure 9, left). The free energy barriers, at $353\,\mathrm{K}$, to get X4-OH and X5-OH are similar: 7.8 and $7.9\,\mathrm{kcal\,mol^{-1}}$ with respect to the reactants, respectively. When addition is carried out by $O(^3P)$, the barriers to get the diradicals X4-O and X5-O are 7.4 and

12

$6.5\,\mathrm{kcal\,mol^{-1}}$ high, respectively. When it is carried out by $H^\bullet$, a barrier of $11.2\,\mathrm{kcal\,mol^{-1}}$ is faced to form the intermediate X4-H, while a barrier of $11.7\,\mathrm{kcal\,mol^{-1}}$ is to be overcome to form X5-H. Regarding the radical adducts so formed, those from OH and $O(^3P)$ attacks have close stabilities $\mathrm{kcal\,mol^{-1}}$: X4-OH (-20.3) and X5-OH (-19.8); X4-O (-19.3) and X5-O (-20.0). The last two could evolve to the same very stable closed shell epoxide $(-80.8\,\mathrm{kcal\,mol^{-1}})$ only upon inter-system crossing [2],[3]. The H radical adducts are somewhat more stable: X4-H and X5-H are both at The H radical adducts are somewhat more stable: X4-H and X5-H are both at $-26.5\,\mathrm{kcal\,mol^{-1}}$.

Hydrogens can be more easily abstracted from one of the two methylenic groups adjacent to the double bond, because an allyl radical system forms. When hydroxyl or the O or H atoms abstract such a hydrogen the allyl radicals X46 and X35 form (Figure 9, right; the two numeric labels indicate the positions of high spin density). H abstraction by OH entails overcoming slightly higher barriers than addition, at this temperature, namely 8.8 and $8.6\,\mathrm{kcal\,mol^{-1}}$, for X35 and X46, respectively. Also X35 and X46 (+ water) are close in free energy, -35.2 and $-35.4\,\mathrm{kcal\,mol^{-1}}$, respectively, and are consequently more stable than their localised counterparts X4-OH and X5-OH. [4]

If H abstraction is carried out instead by atomic oxygen, 8.7 and $10.4\,\mathrm{kcal\,mol^{-1}}$ are the G barrier heights to get X35 and X46 plus $^\bullet$OH. The relevant step free energies (allyl radical + plus OH) are -21.4 and $-21.6\,\mathrm{kcal\,mol^{-1}}$, respectively. When H abstraction is operated by atomic hydrogen, the barrier to get X35 is $13.5\,\mathrm{kcal\,mol^{-1}}$ high, while that for X46 is $13.9\,\mathrm{kcal\,mol^{-1}}$ high. The step free energies (allyl radical + plus H_2) are -20.9 and $-21.0\,\mathrm{kcal\,mol^{-1}}$, respectively.

The radical intermediates of Figure 9 (all referred to collectively as $X^\bullet$) can be involved in a variety of reactions. Some are briefly listed in its lower part. Further radical addition to X itself will produce a new, larger radical, apt to prolong the radical reaction chain or give a closed shell "dimer"[5] via H abstraction (with propagation). If a radical $X^\bullet$ gives H abstraction from X, regeneration of a closed shell species (with propagation) can also occur. Finally, $X^\bullet$ radicals could also add O_2 (propagation) or OH (termination). Another termination could be the coupling of two initial $X^\bullet$ radicals.

The coupling could involve $X^\bullet$, OH, or H moieties. Some of these outcomes will be illustrated in the following sections, operating some selection because of the obviously unmanageable proliferation of possible pathways. We can also add that a further OH addition to the $X^\bullet$ radicals would very easily generate diols, further H addition or H abstraction alcohols (see for instance Figure 6 in [62]). Since H abstraction would generate X again, or an isomer of X if operated by X46 or X35, and a radical among those already considered, it seems less interesting.

Radical addition to give "dimers" $X^\bullet$ radical attacks on positions of the original ester X can then considered, involving the initial radicals derived from hydroxyl attack (addition to the dienic ester are not considered). One kind can be conducted by the intermediate radicals (X4-OH or X5-OH) produced by the hydroxyl addition to the double carbon-carbon bond of X. Another one can be conducted by the radicals generated by H abstraction from X (X46 or

---

[2]An estimate of the half-life for the hydroxyl radical or atomic oxygen, for either addition or H abstraction in step 1 (Figure 9) is, for both, $t_{1/2}=10^{-10}$ to 10^{-11} s, where $t_{1/2} = 1/(k_1 \cdot [\mathrm{ester}])$.

[3]The estimate is based on an assumed ester concentration of $2.8\,\mathrm{M}$, equivalent to a density $\rho=0.88$. This value seems to be consistent with the value reported in the literature. [62]

[4] Two other H abstractions by hydroxyl have been studied. One can occur from the methylene group adjacent to the carbonyl. Its barrier is $11.8\,\mathrm{kcal\,mol^{-1}}$, slightly higher than those just mentioned. The resulting enolic radical intermediate is at $-24.9\,\mathrm{kcal\,mol^{-1}}$, with respect to the same reactants. Another H abstraction from the methoxy group presents a barrier of $11.5\,\mathrm{kcal\,mol^{-1}}$, and a step free energy difference of $-18.3\,\mathrm{kcal\,mol^{-1}}$.

[5]We refer loosely to the addition products as "dimers", though these structures are built from two moieties, of which one is X, while the other $X^\bullet$ is obviously only X-like, because either has one $^\bullet$OH more (from X4-OH and X5-OH), or one hydrogen less than X (from X46 and X35).
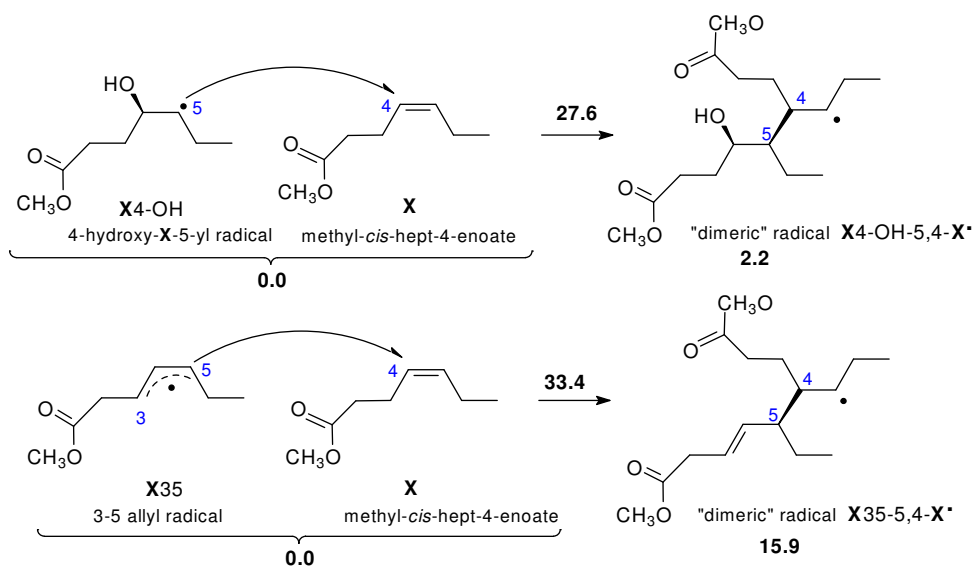
Figure 10: Two radical additions of the initial radicals X4-OH (one out of two) and X35 (one out of four) onto the C=C bond of ester X, to produce "dimers" not containing the peroxy group.
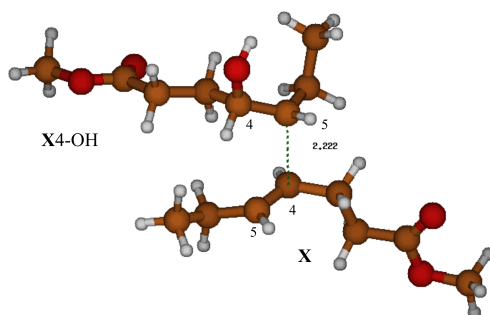

Figure 11: Transition structure for the addition of X4-OH (unpaired electron on C5) to X (C4 attacked), on the way to the radical adduct X4-OH-5,4-X•, representative of the dimers. The unpaired electron will become localised on the original position 5 of X.

X35). Since several possibilities are present (additions, H abstractions), only an illustration of the addition modes will be offered by selecting (1) only one attacking radical of each kind (e.g. X4-OH and X35) among those described in the preceding section, and (2) only one position of addition to the unsaturated systems, namely the C=C carbon closest to the ester group. These addition choices are presented in Figure 10.

One dimer will come from addition of X4-OH (involving its position 5) to position 4 of X. The relevant transition structure Figure 11 corresponds to a barrier of $27.6\,\mathrm{kcal\,mol^{-1}}$. The resulting radical adduct, labelled X4-OH-5,4-X•, carries the unpaired electron obviously localised on the original position 5 of X•. It is located at $2.2\,\mathrm{kcal\,mol^{-1}}$ making reference to X4-OH and X. The other dimer comes similarly from the addition of the more stable radical X35 to X. Its transition structure (Figure 12) is related to a barrier of $34.1\,\mathrm{kcal\,mol^{-1}}$. The adduct is at $15.9\,\mathrm{kcal\,mol^{-1}}$ with respect to the two reacting species. If we consider just the addition step from the adduct X4-OH• and the ester X to give the "dimer" X4-OH-5,4-X•($\Delta G^{\ddagger}$=27.6 kcal mol^{-1}), or that from the adduct X35 with X to give the "dimer" X35-5,4-X• ($\Delta G^{\ddagger}$=33.4 kcal mol^{-1}), we can roughly estimate $t_{1/2}$. "Dimers" of this kind appear to
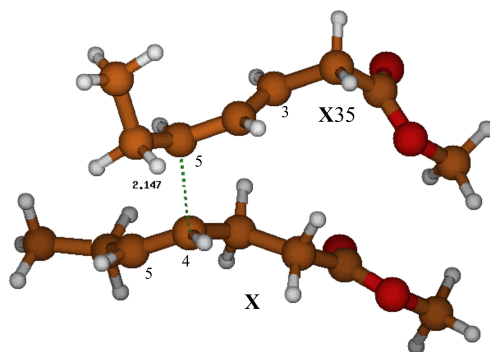
Figure 12: Transition structure for the addition of X35 (allyl radical system on C3-C5) to X (C4 attacked), to give the radical adduct X35-5,4-X$^\bullet$; the unpaired electron will become localised on the original position 5 of X.
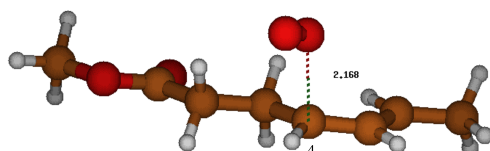

Figure 13: Transition structure for dioxygen addition to C4 of X46, to give the peroxyl radical adduct X46-4-OO$^\bullet$.

have a chance to form, notwithstanding the sizeable barriers (discussed in the Supplemental Information, Section A). This is due to the high X concentration (see footnote 3), with estimated half-life times for the precursor radicals of the order of one minute (making reference to Figure 11) up to one day (Figure 12).

Dioxygen additions to the intermediate radicals.   Going back to the initial intermediates of Figure 9, some dioxygen attacks on them have been studied. Two additions to the localised electron sites in X4-OH and X5-OH give peroxyl groups in position 5 or 4. The peroxyl radicals X4-OH-5-OO$^\bullet$ and X5-OH-4-OO$^\bullet$ form without any energy barrier, and have close stability, $-18.8\,\mathrm{kcal\,mol^{-1}}$, taking as a reference $^3O_2$ plus X4-OH or X5-OH, respectively.

Other four dioxygen attacks on the terminal allylic positions in X46 or X35 are conceivable, of which only two have been examined. The free energy barriers for $^3O_2$ addition to the π-delocalised systems, at $353\,\mathrm{K}$, are similar: 12.6 and $11.2\,\mathrm{kcal\,mol^{-1}}$, respectively.

The stabilities of the two peroxyl radicals so obtained, X46-4-OO$^\bullet$ (Figure 13) and X35-5-OO$^\bullet$, are -7.3 and $-6.4\,\mathrm{kcal\,mol^{-1}}$, again with respect to the reacting species, $^3O_2$ and X46 or X35. [6]

Following O_2 addition, any viable H abstraction by the ROO$^\bullet$ radical would generate a hydroperoxide (and another radical). ROOH is considered as an important intermediate, whose thermal or photochemical decomposition to RO$^\bullet$ + $^\bullet$OH is known to be important for chain branching and oxidation acceleration (see Figure 12 in [64]). However, ROO$^\bullet$ is also known to be a reluctant H abstractor, though abstraction rates increase with temperature (see 3.1.1 [64]). Also peroxyl radical recombination is to be taken into account, though Schaich reports that only for oleic acid peroxyl radical recombination is a major reaction, with the formation of "Russell products". For a discussion of the mechanism of peroxyl radical re-

---

[6]In principle, the two peroxyl radicals, having the oxygen bound either to C4 or to C5, can interconvert via a [2,3] sigmatropic shift. The rearrangement would form a new C-O bond involving the other terminal allylic carbon and a shift of the C=C bond, which could also change from *cis* to *trans*. [37,63] However, the interconversion TS we have found lies at high energy, $+32.8\,\mathrm{kcal\,mol^{-1}}$.
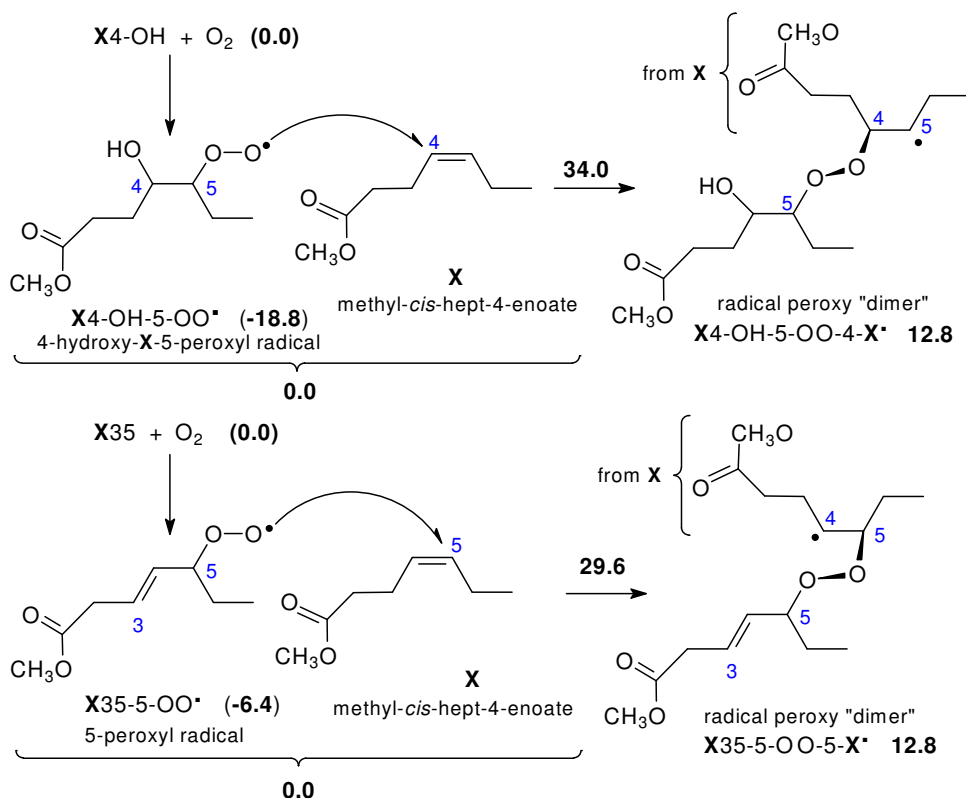
15

Figure 14: Peroxyl radical additions onto the C=C bond of ester X, to produce "dimers" containing a peroxy bridge, X4-OH-5-OO-4-X• and X35-5-OO-5-X•.

combination (self-reaction) and the role of the tetroxide.[65] Its role, in our case, might be a contribution to alkoxyl radicals formation and propagation (see Equation 51 in [64]), together with the production of closed shell alcohols and carbonyl compounds.

Additions involving the peroxyl radicals. Following dioxygen addition, the peroxyl radicals can add to the unsaturation of the original ester. Its outcome is experimentally known and can contribute, more than to the pool of "dimers", to a real branching (compare Equation 48 and 49 in [64]). For instance, one "peroxy dimer" will come from the addition of the terminal oxygen of X4-OH-5-OO• to position 4 of X (Figure 14). The relevant transition structure (Figure 15) corresponds to a barrier of $34.0\,\text{kcal}\,\text{mol}^{-1}$ with respect to the peroxyl radical plus ester reference. The resulting radical adduct, labeled X4-OH-5-OO-4-X•, has the unpaired electron obviously localised on the original position 5 of X. It is located at $12.8\,\text{kcal}\,\text{mol}^{-1}$ making reference to X(4)-OH-5-OO• and X. Another route to a similar kind of "dimer" goes through the addition of X35-5-OO• to X.

Its transition structure (Figure 16) is related to a barrier of $29.6\,\text{kcal}\,\text{mol}^{-1}$, and the adduct is at $12.8\,\text{kcal}\,\text{mol}^{-1}$, both values taken with respect to the two reacting species. Also the formation of peroxy "dimers" presents sizeable barriers, but they could possibly form, due to the high X concentration, with estimated half-life times for the precursor radicals of the order of a few minutes (making reference toFigure 16), or somewhat more than two days for the attack by X35-5-OO•. However, the relative ease by which they split via -O-O- bond cleavage can explain why they are not detected (see Fragmentations section).
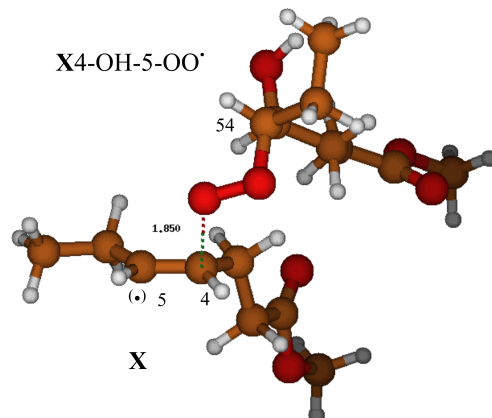
16

Figure 15: TS for the addition of the peroxyl radical X4-OH-5-OO$^\bullet$ to X (at C4), to give the radical adduct X4-OH-5-OO-4-X$^\bullet$; the unpaired electron will be localised on the original position 5 of X.
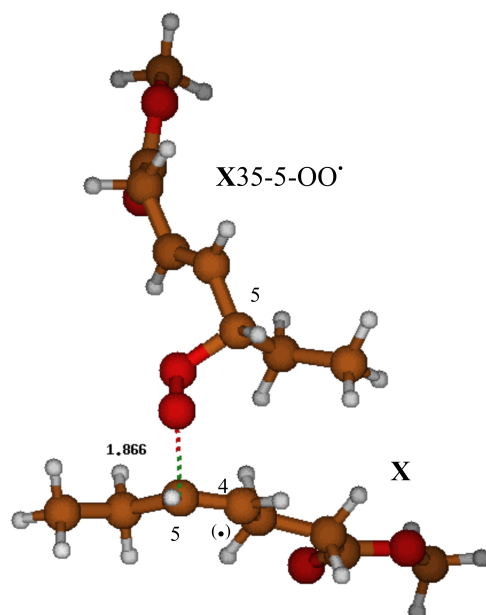

Figure 16: TS for the addition of the peroxyl radical X35-5-OO$^\bullet$ to X (C5), to give the radical adduct X35-5-OO-5-X$^\bullet$. The unpaired electron becomes localised on the original position 4 of X.

17

Radical couplings. Taking the hydroxyl radical (X4-OH or X5-OH) adduct as an example, we can try to assess tentatively how likely will be the formation of "dimers". By considering the absence of structural affinity between the hydroxyl radical and the ester molecules in bulk, we can surmise that diffusion of OH into the liquid phase will not be fast. On this basis, we can then conjecture that the reaction between the ester molecules and OH (reaction 1) will take place chiefly at the gas-liquid interface. By contrast, the initial radical intermediates of the type X-OH of Figure 9 will be structurally similar to the bulk molecules, and, after formation by surface reaction, can be believed to undergo prompt diffusion into the liquid. There, they will react to give "dimers" either with the closed shell esters X (reaction 2) (favoured by the high X concentration), or within themselves via radical couplings (reaction 2') (favoured by the very high rate constant).[7] Though both processes can be conceived as possible, if we accept to consider reaction 1 as taking place mainly at the interface, we can conclude that X-OH will more easily encounter a X molecule than another X-OH radical.

Fragmentations. The possible decomposition of intermediates through β-fragmentation has been considered as a possible source of lighter molecules. Several fragmentations can be imagined, starting from the intermediates discussed so far, to give oxidised and non-oxidised species. Two of them have been selected to exemplify the process. The first one (Figure 17a) is the fragmentation of one initial radical adduct, X5-OH, to give $CH_3O(CO)CH-2^\bullet$ (a vinoxyl-type radical) + $H_2C=CH-CHOH-C_2H_5$. The G barrier is $25.1\,\mathrm{kcal\,mol^{-1}}$, with respect to X5-OH, and the two fragments lie at $7.1\,\mathrm{kcal\,mol^{-1}}$ above it. It does not seem too promising.

For a second case, (Figure 17b) the -O-O- bond cleavage has been first studied in X4-OH-5-OO-4-X$^\bullet$ to get the X4,5-O closed shell epoxide on one side (a well-known kind of product, also observed in this study), and the X4-OH-5-O$^\bullet$ alkoxyl radical on the other side, **(1)**. The transition structure corresponds to a barrier of $13.5\,\mathrm{kcal\,mol^{-1}}$. The two fragments, X4,5-O (the epoxide) and X4-OH-5-O$^\bullet$ are at $-42.7\,\mathrm{kcal\,mol^{-1}}$. The X4-OH-5-O$^\bullet$ alkoxyl radical can also be thought of as formed upon O atom addition to position 5 of the initial X4-OH adduct, **(2)**. Another origin of such an oxyl radical could be the fragmentation of the X4-OH-5-OOH hydroperoxide. If an H abstraction by a X4-OH-5-OO-4-X$^\bullet$ -type intermediate (with the formation of another radical R$^\bullet$) occurred before the -O-O- bond cleavage, a similar step would produce two alkoxyl radicals (plus R$^\bullet$) and enhance the oxidation rate, being an example of bimolecular (peroxyl radical induced) decomposition. From X4-OH-5-O$^\bullet$, formed in either way, different smaller molecules can be subsequently obtained through β-fragmentation. Of the possible fragmentation modes, the most promising is the C4-C5 bond cleavage (G barrier: $2.9\,\mathrm{kcal\,mol^{-1}}$), which gives the radical R, stabilized by α-effect (that can obviously further evolve) and propanal (products at $-16.2\,\mathrm{kcal\,mol^{-1}}$). In lipid oxidation, β-fragmentation is known to correspond to the most important formation channel for aldehydes.[64] The X4-OH-5-O$^\bullet$ alkoxyl radical could also abstract a hydrogen to form a diol. This process exemplifies how the pool of oxidised derivatives can diversify, exhibiting not only increase but also a decrease in molecular weight, all known features of lipid oxidation.

3.4.2 The "linoleate model": H abstraction.

The hydroxyl radical can very easily abstract one bis-allylic H from the methylenic group in between the two double bonds of methyl-*cis,cis*-deca-4,7-dienoate (Y). The abstraction entails, at the experiment temperature, overcoming a barrier of $8.7\,\mathrm{kcal\,mol^{-1}}$ (Figure 18 and 19).

---

[7] As a simple example, for the radical coupling $C_2H_5 + C_2H_5 \rightarrow$ n-C_4H_{10}, k values in the range 7.8×10^9 - $1.6 \times 10^{10}\,\mathrm{M^{-1}\,s^{-1}}$ are reported.[66,67]
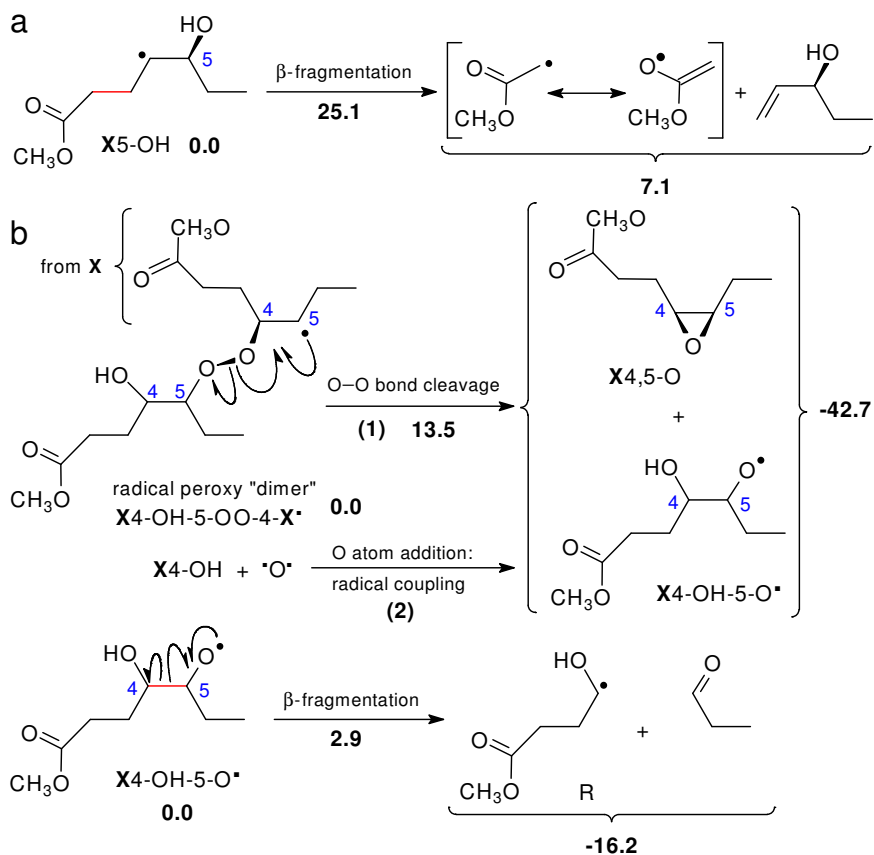
Figure 17: Examples of formation of lighter molecules. (a) β-fragmentations in one initial adduct. (b) From the dimer X4-OH-5-OO-4-X•, an oxyl radical X4-OH-5-O• can form upon O-O bond cleavage (the same radical could come from X4-OH, through O atom addition). Then, the radical R and propanal can form upon C-C bond cleavage (β-fragmentations).
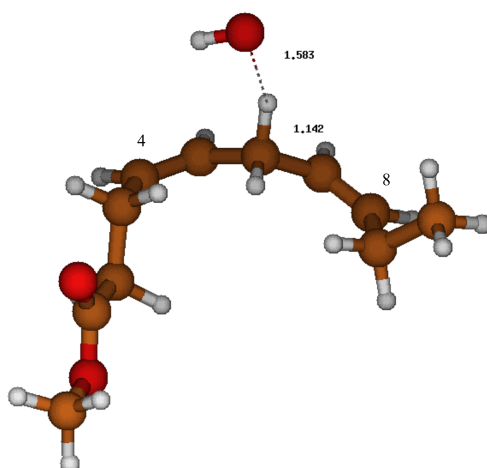

Figure 18: Transition structure for H abstraction by the hydroxyl radical from the model methyl-*cis,cis*-deca-4,7-dienoate. A pentadienyl radical π-system forms, stretching from C4 to C8, Y48.
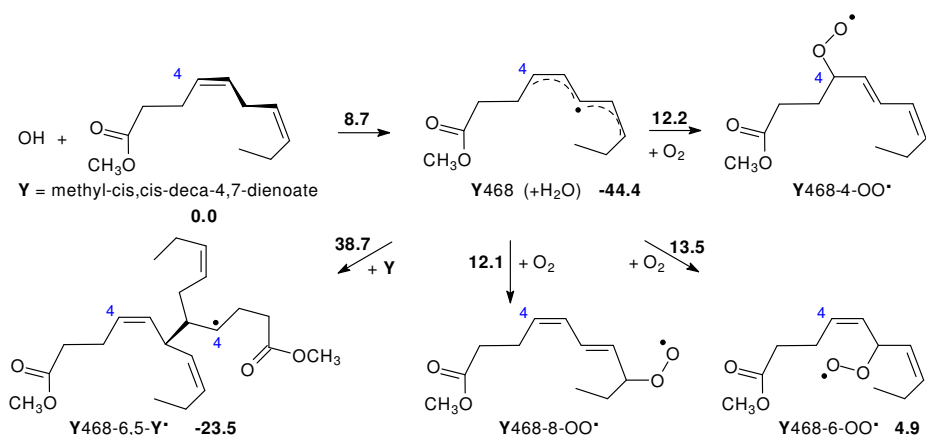
Figure 19: H abstraction operated by the hydroxyl radical from the bis-allylic position of methyl-*cis,cis*-deca-4,7-dienoate (Y). Subsequent "dimers" formation by radical addition to Y (left), or O_2 additions to the pentadienyl radical system (right).

The intermediate product, a delocalised pentadienyl radical, is located at $-44.4 \, \text{kcal mol}^{-1}$ (water added) with respect to the reactants. The pentadienyl π-system is characterised by higher spin densities on the central carbon and the two extreme carbons. The values are: 0.505, on C4; 0.620, on C6, central carbon of the pentadienyl radical system; 0.502 on C8 (then -0.272 on C5 and -0.267 on C7). This radical can subsequently add to another Y molecule or X (but mixed adducts are not considered in this study), to give a "dimer" that does not contain extra oxygens with respect to the original molecules. The relevant barrier for addition to Y carried out by the highest spin density carbon, C6, is $38.7 \, \text{kcal mol}^{-1}$ high, and the dimer is located at $23.5 \, \text{kcal mol}^{-1}$. Alternatively, the pentadienyl radical can first undergo dioxygen addition. Addition can take place on each of the three high-spin density positions, C4, C6, and C8. The G barriers have similar height: 12.2 (C4), 13.5 (C6), and 12.1 (C8) kcal mol^{-1}, with a slight preference for the external positions of the pentadienyl radical (with the formation of conjugate diene bonds), in spite of the higher spin density on the central carbon. The peroxyl radical formation appears to be in itself reversible, because the backwards step requires overcoming barriers of ca. $7.8 \, \text{kcal mol}^{-1}$ only.

Subsequently, the peroxyl radical so obtained can carry out a radical attack with its terminal oxygen on the same dienoate Y together with a variety of other reactions. If the addition of a radical occurred on one terminal carbon of the pentadienyl radical system, it would produce a closed shell intermediate with conjugated double bonds (thermodynamically more stable than two isolated C=C bonds), but with known enhanced attitude to undergo radical addition with respect to one isolated double bond. For linoleate, addition is indeed known to gain importance past the initial stages of oxidation (see p. 329 of [64]).

Our bis-allylic H abstraction barrier ($\Delta G^{\ddagger} = 8.7 \, \text{kcal mol}^{-1}$) can be compared with the values computed by Tejero et al.[29] [Table 1: MPWB1K: 11.2; B3LYP: 7.7 ("underestimates"); BH&HLYP: $15.0 \, \text{kcal mol}^{-1}$ ("overestimates")]. Also our barrier for dioxygen addition, $20.2 \, \text{kcal mol}^{-1}$, compares with their Table 2 values (MPWB1K: 17.7; B3LYP: 15.1; BH&HLYP: $24.4 \, \text{kcal mol}^{-1}$).

4 Discussion

In this section, we try to interpret experimental findings. In particular, we focus on the striking differences between He-H$_2$O and He-O$_2$. The latter is considered as a reference case in which the concentration of both OH and H is negligible. Finally, we try to understand the meaning of the correlation between the conversion of unsaturated FAMEs and OH exposure shown in Figure 6. If we consider the computational results for the initial steps (OH, H, and O atom attacks to the esters) we see that addition prevails onto allylic-H abstraction for the oleate model (one isolated double bond). In the case of the linoleate model attacked by OH, a slightly lower G barrier is found for abstraction of the bis-allylic hydrogen. As a conclusion and starting point of the following discussion, we underline that O and OH can carry out an addition to the double bond with similar efficiency and both more efficiently than the H atom. As a consequence, the relative importance of OH or O in the initial reaction steps depends only on their concentration in the jet, which determines the total amount of reactants impinging on the oil surface in the treatment time.

Volatile products Fragmentation processes can produced lighter products. Bond cleavages can either regard peroxy compounds (the RO-OR' bond is characterized by a D$_e$ value of only 47-48 kcal mol^{-1}, hence is per se a weak bond with respect to homolysis), or β-fragmentations triggered by the formation of radicals of suitable structure, in particular alkoxyl radicals. One example of the former can be the O-O bond cleavage illustrated by Figure 17 (not a sheer cleavage, because an epoxide forms). For instance, in Figure 17 the O-O bond cleavage G barrier, with concomitant C-O bond formation, is only 13.5 kcal mol^{-1} high. One example of the latter is the X4-OH-5-O$^\bullet$ alkoxyl radical, again in Figure 17: the β-fragmentation involving its C4-C5 bond is quite easy, $\Delta G^{\ddagger}$= 2.9 kcal mol^{-1}. One of the products is an aldehyde, the other, R, can be envisaged, from the point of view of volatile product formation, as a precursor of a hydroxy- or oxo- ester, depending on which hydrogen might be abstracted (from C3-H or from –OH).

About 50% or even more of C18$_U$ conversion goes into volatile products (see Figure 7) with He-H$_2$O gas feed. In such a condition, and according to the model results,[22] the O concentration is just about a factor of two lower than that of OH. We are then in the impossibility of discriminating between OH and O as the main precursor of volatile products, neither on the basis of the concentrations nor by looking at the products in detail. We conclude that OH is not the dominant source of volatile products since O might give a contribution of the same order of magnitude.

Dimers The presence of "dimers" could be illustrated by processes as those shown in Figure 10 and 14, and also by the occurrence of radical coupling between intermediate radicals. By the theoretical results, we would be inclined to exclude a significant presence of peroxy "dimers", such as those shown in Figure 14, because of their rather easy fragmentation (in fact, they are not detected in the present experiment). Conversely, the addition steps of Figure 10 present high free energy barriers that seem to prevent the formation of the radical "dimers". However, by taking into account the very high concentration of X itself, the estimated rate constants lead to an assessment of t$_{1/2}$ (for the radicals X4-OH or X35) of the order of tens of seconds, in the case of X4-OH-5,4-X$^\bullet$ formation, and ca. 10^5 s (i.e. one day) for X35-5,4-X$^\bullet$ formation. As said, another source of "dimers" could be the radical coupling of two intermediate species (as those of Figure 9). Its importance is quite hard to assess.

The three reactants OH, H and O are all possible precursors of the radical chain C18. The question is then why the dimerization process occurs only in the He-H$_2$O jet, and not in the He-O$_2$ case, in which high O concentrations are expected. We note that in the latter case an abundant O$_2$ flux (orders of magnitudes larger than that of OH, H and O) flows onto

21

the sample. The addition of O_2 onto the radical centres, inhibits the formation of dimers as in Figure 9, leading to the formation of ROO. Afterwards, the latter can either abstract H, resulting in an ROOH, or attack one X giving a peroxy-dimer, which in turn easily breaks due to the weakness of the O-O bond. In conclusion the abundance of O_2 stops the formation of dimers.

Reduced chains The presence of reduced C18 chains could be traced back to the very beginning of the reaction sequences, i.e. to hydrogen atom addition to X to form radicals as X4-H or X5-H, shown in Figure 9. To get C18 H-saturated chains, these radicals should, in turn, perform H abstraction, possibly from the high-concentration closed shell molecules surrounding them. The second step would be akin to those leading to X46 or X35, so forming reduced C18 chains with propagation. An alternative could be a radical coupling with an H atom.

The presence of reduced chains is then an evidence of abundant H presence in the He-H_2O jet. Reduced chains are the end product of about 10-15% of the converted $C18_U$. Their increase on increasing OH exposure implies that H exposure is increasing accordingly.

Oxidized chains Making reference again to Figure 9, initial radical adducts bearing either an OH substituent, or diradicals bearing an $O^\bullet$ substituent, both could evolve through O atom or OH further additions (radical couplings). In the former case, a subsequent H abstraction would be required to obtain a closed shell product. An alternative would be an H abstraction to produce oxidised closed shell species. In the case of formation of X4-O or X5-O, H abstraction from the carbon bearing the oxyl substituent, a radical precursor of a ketoester would form. Upon inter-system crossing in the triplet $X4-O^\bullet$ or $X5-O^\bullet$ radicals, an epoxide would instead form.

For this class of products, the same considerations hold as those relevant to volatile products. As a matter of fact, we cannot attribute a dominance to any of the oxidising agents for the first reaction steps. The substantial products similarity between the two gas feed cases is not of help for a discrimination of the initial step since the final products can be the result of many complex further steps after the first one. We conclude, again, that we have no evidence of a predominance of OH as a precursor of oxidised chains.

Conversion vs. OH exposure In summary, none of the products classes can be ascribed predominantly to OH attack, but rather to a sum of contributions whose relative weights are out of the range of our present knowledge. Thus, the apparent correlation between $C18_U$ conversion and OH exposure shown in Figure 6 is not a proof of the dominance of OH in the initiation of conversion reactions. The same holds for the individual product classes reported in Figure 7. Rather, OH exposure comes out to be representative of the exposure to the whole ensemble of plasma generated OH, H, O and, eventually further ROS. OH exposure increase, we recall, is obtained in two ways. One way is to increase the treatment time. In such a way the relative amount of active plasma species remains unchanged. The other way is to increase the discharge power, by which an increase of the concentration of all the active species in the plasma jet is reasonably expected. The measurement of OH concentration by LIF, then, does not bring to the assessment of a quantitative relationship between OH and conversion products. The support of LIF investigations is, nevertheless still very important. First, it characterises the condition of OH (and H) flux as being much higher than that of previous studies.[25] Second, it shows that the air intake at the jet-target interface is negligible, thus ensuring an air-free condition treatment for the He-H_2O.

5 Conclusions

The present joint experimental and theoretical study allows drawing some general conclusions whose interest is manifold, according to their utilisation in a fundamental or applicative context. OH and O cannot be discriminated as oxidation precursors in a condition in which their concentrations are comparable, since the barriers of their initial reaction steps are very similar, and the routes driving to the final products are too much complex and mostly unknown. From a fundamental point of view, a possible progress would require the availability of intense sources of single species; that is not possible at present using conventional plasma sources. From an applicative point of view, if the scope is simply the FAME oxidation, the non-selectivity of the plasma-jet source does not appear to be a real problem. Also, the use of O_2 addition in place of H_2O is advantageous for achieving a much faster process.

FAME reduction is, on the contrary, quite well assessed as due to H addition. A general lesson we have learned is that the water containing plasma jet acts, at the same time, as both an oxidising and reducing agent. Further studies might be conceived with just H_2 only addition to the gas feed, and a quantification of the H flux by (TALIF).

Useless to say, such a complex system requires a big effort, both experimental and theoretical, to gain true knowledge. We underline that, without model calculations, the apparent C18 conversion vs. OH exposure correlation is highly susceptible of being erroneously interpreted as a dominant role of OH, in particular in oxidation processes.

We finally observe that the present work has a natural placement in the plasma medicine context, but we like to think that, together with the challenge of more radical-selective plasma sources, it might open new ways for a fundamental understanding of chemical-induced lipid oxidation mechanisms.

References

[1] Wenk, M. R. *Cell* **2010**, *143*, 888 – 895.

[2] Pohl, C. H.; Kock, J. L. *Molecules* **2014**, *19*, 1273.

[3] Yin, H.; Xu, L.; Porter, N. A. *Chem. Rev.* **2011**, *111*, 5944–5972.

[4] Graves, D. B. *J. Phys. D: Appl. Phys.* **2012**, *45*, 263001.

[5] Winter, J.; Brandenburg, R.; Weltmann, K.-D. *Plasma Sources Sci. Technol.* **2015**, *24*, 064001.

[6] Frankel, E. N. *Lipid oxidation;* Woodhead Publishing, 2005.

[7] Morales, A.; Marmesat, S.; Dobarganes, M. C.; Márquez-Ruiz, G.; Velasco, J. *J. Chromatogr. A* **2012**, *1254*, 62 – 70.

[8] Nuñez, A.; Foglia, T. A.; Piazza, G. J. *Lipids* **2001**, *36*, 851–856.

[9] Katusin-Razem, B.; Razem, D. *J. Phys. Chem. A* **2000**, *104*, 1482–1494.

[10] Wang, X.-H.; Ohshima, T.; Ushio, H.; Koizumi, C. *Lipids* **1999**, *34*, 675–679.

[11] Cosgrove, J. P.; Church, D. F.; Pryor, W. A. *Lipids* **1987**, *22*, 299–304.

[12] Labuza, T. P.; Tsuyuki, H.; Karel, M. *J. Am. Oil Chem. Soc.* **1969**, *46*, 409–416.

[13] Bax, S.; Hakka, M. H.; Glaude, P.-A.; Herbinet, O.; Battin-Leclerc, F. *Combust. Flame* **2010**, *157*, 1220 – 1229.

[14] Tedetti, M.; Kawamura, K.; Narukawa, M.; Joux, F.; Charrière, B.; Sempéré, R. *J. Photoch. Photobio. A* **2007**, *188*, 135 – 139.

[15] Neff, W. E.; Frankel, E. N.; Selke, E.; Weisleder, D. *Lipids* **1983**, *18*, 868–876.

[16] Choe, E.; Min, D. B. *Compr. Rev. Food Sci. F.* **2006**, *5*, 169–186.

[17] Bogaerts, A.; Yusupov, M.; Van der Paal, J.; Verlackt, C. C. W.; Neyts, E. C. *Plasma Process. Polym.* **2014**, *11*, 1156–1168.

[18] Yusupov, M.; Neyts, E. C.; Verlackt, C. C.; Khalilov, U.; van Duin, A. C. T.; Bogaerts, A. *Plasma Process. Polym.* **2015**, *12*, 162–171.

[19] Van der Paal, J.; Verlackt, C. C.; Yusupov, M.; Neyts, E. C.; Bogaerts, A. *J. Phys. D: Appl. Phys.* **2015**, *48*, 155202.

[20] Fridman, A.; Friedman, G. *Plasma Medicine;* Wiley, 2013.

[21] Scapinello, M.; Martini, L. M.; Tosi, P.; Maranzana, A.; Tonachini, G. *RSC Adv.* **2015**, *5*, 38581–38590.

[22] Naidis, G. V. *Plasma Sources Sci. Technol.* **2013**, *22*, 035015.

[23] McKay, K.; Liu, D. X.; Rong, M. Z.; Iza, F.; Kong, M. G. *J. Phys. D: Appl. Phys.* **2012**, *45*, 172001.

[24] Naidis, G. V. *Plasma Sources Sci. Technol.* **2014**, *23*, 065014.

[25] Van Durme, J.; Nikiforov, A.; Vandamme, J.; De Winne, A.; Leys, C. *Food Res. Int.* **2014**, *62*, 868–876.

[26] Vandamme, J.; Nikiforov, A.; Dujardin, K.; Leys, C.; Cooman, L. D.; Van Durme, J. *Food Res. Int.* **2015**, *72*, 115 – 125.

[27] Vandamme, J.; Nikiforov, A.; Roose, M. D.; Leys, C.; Cooman, L. D.; Van Durme, J. *Food Res. Int.* **2016**, *79*, 54 – 63.

[28] Van Durme, J.; Vandamme, J. *Food Chem.* **2016**, *208*, 185 – 191.

[29] Tejero, I.; Gonzalez-Lafont, A.; Lluch, J. M.; Eriksson, L. A. *J. Phys. Chem. B* **2007**, *111*, 5684 – 5693.

[30] Tejero, I.; Gonzalez-Lafont, A.; Lluch, J. M.; Eriksson, L. A. *Chem. Phys. Lett.* **2004**, *398*, 336–342.

[31] Olivella, S.; Solé, A. *J. Am. Chem. Soc.* **2003**, *125*.

[32] Sobolewski, M. A. *J. Vac. Sci. Technol., A* **1992**, *10*, 3550–3562.

[33] Hofmann, S.; van Gessel, A. F. H.; Verreycken, T.; Bruggeman, P. *Plasma Sources Sci. Technol.* **2011**, *20*, 065010.

[34] Dilecce, G.; Martini, L. M.; Tosi, P.; Scotoni, M.; Benedictis, S. D. *Plasma Sources Sci. Technol.* **2015**, *24*, 034007.

[35] Scanlon, J. T.; Willis, D. E. *J. Chromatogr. Sci.* **1985**, *23*, 333–340.

[36] Robert G Parr, W. Y. *Density-functional theory of atoms and molecules;* Oxford University Press, 1989.

[37] Zhao, Y.; Truhlar, D. G. *Theor. Chem. Acc.* **2008**, *120*, 215–241.

[38] Schlegel, H. B.; Springer Netherlands, 1981; pages 129–159; NATO Advanced Study Institutes Series 67, 1 ed.

[39] Schlegel, H. B. *J. Chem. Phys.* **1982**, *77*, 3676–3681.

[40] Schlegel, H. B. *J. Comp. Chem.* **1982**, *3*, 214–218.

[41] Schlegel, H. B.; Binkley, J. S.; Pople, J. A. *J. Chem. Phys.* **1984**, *80*, 1976–1981.

[42] Pople, J. A.; Gill, P. M.; Johnson, B. G. *Chem. Phys. Lett.* **1992**, *199*, 557 – 560.

[43] Kendall, R. A.; Dunning, T. H.; Harrison, R. J. *J. Chem. Phys.* **1992**, *96*, 6796–6806.

[44] Zhao, Y.; Truhlar, D. G. *Accounts Chem. Res.* **2008**, *41*, 157–167.

[45] Trogolo, D.; Maranzana, A.; Ghigo, G.; Tonachini, G. *J. Phys. Chem. A* **2014**, *118*, 427–440.

[46] Marenich, A. V.; Cramer, C. J.; Truhlar, D. G. *J. Phys. Chem. B* **2009**, *113*, 6378–6396.

[47] Tomasi, J.; Mennucci, B.; Cancès, E. *J. Mol. Struc.- Theochem* **1999**, *464*, 211 – 226.

[48] Gunstone, F.; Harwood, J.; Padley, F.; Taylor & Francis, 1994; page 437; Chapman & Hall chemical database.

[49] Fasman, G. *Practical Handbook of Biochemistry and Molecular Biology;* CRC Press, 1989.

[50] Hehre, W. J.; Radom, L.; Schleyer, P. v. R.; Pople, J.; Wiley, 1986; chapter 6.3; A Wiley-Interscience publication.

[51] Vibrational Analysis in Gaussian. Ochterski, J. W. http://www.gaussian.com/g_whitepap/vib.htm, **1999**.

[52] Thermochemistry in Gaussian. Ochterski, J. W. http://www.gaussian.com/g_whitepap/thermo.htm, **2000**.

[53] Eyring, H. *J. Chem. Phys.* **1935**, *3*, 107–115.

[54] Evans, M. G.; Polanyi, M. *Trans. Faraday Soc.* **1935**, *31*, 875–894.

[55] Laidler, K. J.; King, M. C. *J. Phys. Chem.* **1983**, *87*, 2657–2664.

[56] Truhlar, D. G.; Garrett, B. C.; Klippenstein, S. J. *J. Phys. Chem.* **1996**, *100*, 12771–12800.

[57] Yamaguchi, K.; Jensen, F.; Dorigo, A.; Houk, K. N. *Chem. Phys. Lett.* **1988**, *149*, 537–542.

[58] Yamanaka, S.; Kawakami, T.; Nagao, K.; Yamaguchi, K. *Chem. Phys. Lett.* **1994**, *231*, 25–33.

[59] Gaussian 09 Revision A.02. Frisch, M. J.; Trucks, G. W.; Schlegel, H. B.; Scuseria, G. E.; Robb, M. A.; Cheeseman, J. R.; Scalmani, G.; Barone, V.; Mennucci, B.; Petersson, G. A.; Nakatsuji, H.; Caricato, M.; Li, X.; Hratchian, H. P.; Izmaylov, A. F.; Bloino, J.; Zheng, G.; Sonnenberg, J. L.; Hada, M.; Ehara, M.; Toyota, K.; Fukuda, R.; Hasegawa, J.; Ishida, M.; Nakajima, T.; Honda, Y.; Kitao, O.; Nakai, H.; Vreven, T.; Montgomery, Jr., J. A.; Peralta, J. E.; Ogliaro, F.; Bearpark, M.; Heyd, J. J.; Brothers, E.; Kudin, K. N.; Staroverov, V. N.; Kobayashi, R.; Normand, J.; Raghavachari, K.; Rendell, A.; Burant, J. C.; Iyengar, S. S.; Tomasi, J.; Cossi, M.; Rega, N.; Millam, J. M.; Klene, M.; Knox, J. E.; Cross, J. B.; Bakken, V.; Adamo, C.; Jaramillo, J.; Gomperts, R.; Stratmann, R. E.; Yazyev, O.; Austin, A. J.; Cammi, R.; Pomelli, C.; Ochterski, J. W.; Martin, R. L.; Morokuma, K.; Zakrzewski, V. G.; Voth, G. A.; Salvador, P.; Dannenberg, J. J.; Dapprich, S.; Daniels, A. D.; Farkas, A.; Foresman, J. B.; Ortiz, J. V.; Cioslowski, J.; Fox, D. J.

[60] Paschke, R. F.; Peterson, L. E.; Wheeler, D. H. *J. Am. Oil Chem. Soc.* **1964**, *41*, 723–727.

[61] Carey, F. A.; Sundberg, R. J. *Advanced Organic Chemistry, Part A: Structure and Mechanisms;* Springer, fifth ed., 2007.

[62] Van Der Paal, J.; Aernouts, S.; van Duin, A. C. T.; Neyts, E. C.; Bogaerts, A. *J. Phys. D: Appl. Phys.* **2013**, *46*, 395201.

[63] Porter, N. A. *J. Org. Chem.* **2013**, *78*, 3511–3524.

[64] Schaich, K. M. In *Bailey's Industrial Oil and Fat Products;* John Wiley & Sons, Inc, 2005; chapter 7.

[65] Ghigo, G.; Maranzana, A.; Tonachini, G. *J. Chem. Phys.* **2003**, *118*, 10575–10583.

[66] Munk, J.; Pagsberg, P.; Ratajczak, E.; Sillesen, A. *J. Phys. Chem.* **1986**, *90*, 2752–2757.

[67] Dobis, O.; Benson, S. W. *J. Am. Chem. Soc.* **1991**, *113*, 6377–6386.

Graphical Abstract

The interaction of radicals with lipids is of paramount importance in different fields ranging from biology to atmospheric chemistry. Fatty acid methyl esters are treated by a plasma jet, while laser induced fluorescence is used to measure the concentration of the hydroxyl radical in the jet, as a partial characterisation of the flux of radicals that induce the lipid reactivity. Theoretical calculations give some hints on the reaction mechanisms.

ToC figure